Charles University in Prague

Faculty of Mathematics and Physics

BACHELOR THESIS

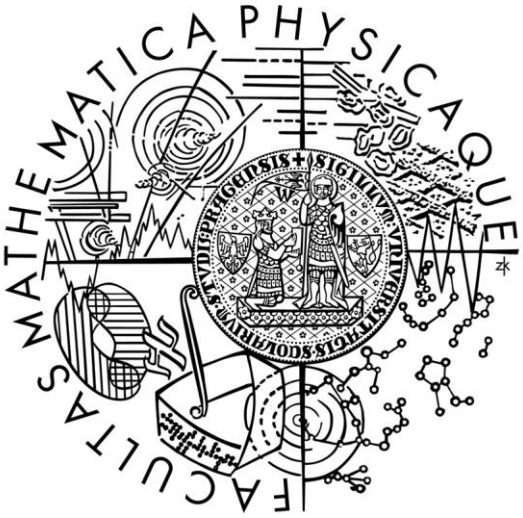

Martin Statelov

Optical characterization of thin oxide layers

Institute of Physics

Supervisor of the bachelor thesis: prof. Ing. Jan Franc, DrSc.

Study program: Physics

Specialization: General physics

Prague 2015

ACKNOWLEGDEMENTS

I would like to thank prof. Ing. Jan Franc, DrSc. and Mgr. Jakub Zázvorka for guidance and assistance during this thesis. I am also grateful to the whole team at the department of semiconductors and semiconductor optoelectronics for technical assistance. Lastly, I wish to thank my family and close relatives for the support that they have provided.

I declare that I carried out this bachelor thesis independently, and only with the cited sources, literature and other professional sources.

I understand that my work relates to the rights and obligations under the Act No. 121/2000 Coll., the Copyright Act, as amended, in particular the fact that the Charles University in Prague has the right to conclude a license agreement on the use of this work as a school work pursuant to Section 60 paragraph 1 of the Copyright Act.

In: …….. Date: …….. Signature: ……..

Názov práce: Optická charakterizácia tenkých oxidových vrstev

Autor: Martin Statelov

Ústav: Fyzikálni ústav UK

Vedouci bakalářske práce: prof. Ing. Jan Franc, DrSc.

Abstrakt: Účinnosť detektorov na báze CdZnTe priamo súvisí s kvalitou povrchu. Mechanické leštenie, chemické leptanie a pasivácia sú bežne používané pre tento účel. Dynamika a vlastnosti CdZnTe povrchových oxidových vrstiev, vytvorených leptaním a pasiváciou v roztokoch KOH a NH_4F/H_2O_2, boli študované pomocou optickej ellipsometrie. Model efektívneho priblíženia média bol použitý na vyhodnocovanie ellipsometrických spektier. Hrúbka a rýchlosť tvorby povrchovej oxidovej vrstvy boli rozdielne pri každej metóde. Zvodové prúdy boli zároveň merané a boli porovnané s vlastnosťami povrchových oxidových vrstiev. NH_4F/H_2O_2 pasivácia sa ukázala ako metóda s najpriaznivemejšimi vlastnostami povrchovej oxidovej vrstvy; hrúba vstva a malé zvodové prúdy.

Klíčová slova: oxidové vrstvy, elipsometrie, voltampérové charakteristiky

Title: Optical characterization of thin oxide layers

Author: Martin Statelov

Institute: Institute of Physics, Charles University

Supervisor of the bachelor thesis: prof. Ing. Jan Franc, DrSc.

Abstract: Performance of CdZnTe-based detectors is highly related to the surface quality. Mechanical polishing, chemical etching and passivation are routinely employed for this purpose. The dynamics and properties of CdZnTe surface oxide layers, created by etching-only and passivation by KOH and NH_4F/H_2O_2 solutions, were studied by optical ellipsometry. Effective medium approximation model was used to evaluate ellipsometric spectra. Thickness and formation rate of the surface oxide layers differed in each of the passivation method. Leakage currents were measured simultaneously and were compared with the surface oxide layer properties. NH_4F/H_2O_2 passivation showed to be method with most desirable properties of the surface oxide layer; thick oxide layer and low leakage currents.

Keywords: oxide layers, ellipsometry, volt-ampere characteristics

Table of Contents

1. Introduction

Semiconductors are the cornerstone of modern technology. Since the development of the first transistor on germanium in 1947, semiconducting materials are the topic of a more focused research with emphasis on applications. The unique distribution of atoms in the material lattice results in forming of the electronic state bands, the valence (last filled with electrons) and the conduction band (empty or partially filled with electrons at temperature 0 K), respectively. Between these bands there is a range of energy states that cannot be occupied with charge carriers, called band gap. Usually the value of band gap for semiconductors is in the range of 0.1 – 3 eV. Materials with band gap above 3 eV are considered to be dielectric. Semiconductors can be elemental materials (silicon or germanium) or compound materials (InP, GaAs, InSb, CdTe etc.). Both groups find various applications e.g. electronics, medical industry, defence and security, sensing and radiation detection. There are two main approaches to detection of hard X-ray and gamma-ray radiation: indirect and direct conversion. Indirect conversion employs materials called scintillators which upon irradiating convert the x-ray and gamma-ray radiation into visible radiation detectable by commonly used photodetectors (e.g. Si-photodiode). Direct detection employs materials that generate electron-hole pairs upon absorbing the incoming radiation that are accelerated in an electric field applied to the detector. The generated charges are collected on metal contacts in the form of a current pulse. The amount of the collected charge is related to the energy of the incoming radiation and the spectrum characteristics of the studied X-ray and/or gamma-ray can be evaluated. Silicon and germanium are good quality radiation detectors, because of their achievable purity. However, their low atomic numbers result in a low attenuation coefficient of high-energy radiation and because of their relatively small band gap they have to be cooled with liquid nitrogen to achieve good spectral resolution. On the other hand, compound materials such as CdTe can operate at room temperature and detect very high-energy radiation due to their large atomic number. Tertiary compound CdZnTe, where the concentration on zinc varies

usually in the range of 0 – 15 %, has a larger bandgap. Both CdTe and CdZnTe find applications in modern computer tomography and radiation monitors. However optimization of their crystal growth, new detector concepts and enhanced detector characterization are still in semiconductor research focus. Dare present in the crystal bulk and on the surface that influence the final detector properties. The parameters of deep energetic levels and surface states are still under study.

1.1. CdTe and CdZnTe

Cadmium telluride (CdTe) is a stable crystalline compound with excellent semiconducting properties; specifically a high (average) atomic number, large band gap and high electron mobility (see Table 1). Semi-insulating CdTe and CdZnTe are important materials for X-ray and gamma ray detection [1]. High resistivity of the material achieved through compensation of shallow defect levels and Fermi energy pinning guarantees a good signal-to-noise ratio of the detectors. These detectors can operate at room temperature. The material can be also used in photovoltaics, as an substrate for epitaxially prepared HgCdTe, that is a detector of infrared radiation, and as an electro-optic modulator.

Lattice constant (300 K)	0.648 nm
Band gap (300 K, direct)	1.5 eV
Atomic number	48 (Cd), 52 (Te)
Electron mobility	1100 cm^2/Vs
Thermal conductivity (300 K)	6.2 Wm/m^2
Resistivity (300 K)	10^9-10^{10} Ω·cm

Table 1: Properties of CdTe. *Source [1]*.

This combination of advantageous properties makes CdTe an excellent detector for medical, security, and astrophysics applications. Despite that, the use of CdTe material is still limited by some important problems such as the presence of secondary phases, impurities, and surface quality. Each of these factors can cause degradation of detector performance.

1.2. Surface quality

The surface quality of CdTe plays an important role in the performance of CdTe based detectors. Usually the effects of surface preparation on the material leakage current are studied through I-V characteristics and photocurrent measurements [2,3,4,5]. Various studies have shown that surface properties of the lateral sides of the detector control many aspects of device operation and performance [6,7,8,9,10]. Mostly used surface preparation is mechanical polishing and chemical etching in bromine-methanol (Br-MeOH) solution [2,3,7]. The surface morphology is usually investigated by XPS and interferometry measurements [11,12,13]. However, because the results even with using the same techniques do vary, the optimization of the surface preparation is still under investigation. Also one of the observed phenomena is the deterioration of the detectors over time after processing. It has been studied with XPS measurements [13,14] that a surface oxide (TeO_2) layer forms after usual etching in Br-MeOH solution. It is believed that this oxide formation is one of the causes of the detector parameters changes and is responsible for its time degradation. To evaluate the oxide layer properties in dependence on surface preparation, XPS and spectroscopic ellipsometry was used [15,16,17]. But no insight into the dynamics of the oxidization was published so far. A way to eliminate the oxidization issue in CdTe/CdZnTe detectors is to passivate the material surface. Results show that KOH and NH_4F/H_2O_2 passivation yields a well-behaved surface [5,7]. However even the passivation influences the detector properties and requires further investigation.

In this thesis we have investigated a formation rate of native oxides and oxides created by passivation processes, and their effects on semiconducting properties. The main goal was to find a surface layer that is stable over a long time period and causes minimum leakage currents. The dynamics and properties of CdZnTe surface were studied by optical ellipsometry and the leakage currents by volt-ampere characteristics. In the theoretical part we explain the fundamental theory of optical properties and polarization, which is crucial for optical characterization. In experimental methods the basic principles of ellipsometry and volt-ampere characteristic

are explained. Then we summarize important properties of our CdZnTe samples and describe surface preparation. In the last part results are presented and discussed.

2. Theoretical Background

2.1. Optical properties of materials

2.1.1. Maxwell's equations and the wave equation

Maxwell's equations are a set of partial differential equations that form the foundation of classical optics. They can be expressed in the differential form [18]:

$$\nabla \cdot \vec{D} = \rho \tag{1}$$

$$\nabla \cdot \vec{B} = 0 \tag{2}$$

$$\nabla \times \vec{E} + \frac{\partial \vec{B}}{\partial t} = 0 \tag{3}$$

$$\nabla \times \vec{H} - \frac{\partial \vec{D}}{\partial t} = \vec{j} \tag{4}$$

where $\vec{E}$ is the electric field, $\vec{D}$ is the displacement field, $\vec{B}$ is the magnetic field, $\vec{H}$ is the magnetizing field, ρ is the charge density, $\vec{j}$ is the current density. To allow a unique determination of the field vectors from a given distribution of currents and charges, these equations must be supplemented by relations, which describe the behaviour of substances under the influence of the field. These relations are known as material equations. In general, they can be complicated. However, if we suppose materials at rest (or very slow speed) and isotropy, then they can be expressed in the simple form [18]:

$$\vec{j} = \sigma \vec{E} \tag{5}$$

$$\vec{D} = \varepsilon \vec{E} \tag{6}$$

$$\vec{B} = \mu\vec{H} \tag{7}$$

Here σ is called the specific conductivity, ε the permittivity and μ the permeability. These parameters describe the conducting, electric and magnetic properties of materials, respectively.

We shall confine our attention to a medium without charges or currents, i.e. $\vec{j} = 0$ and $\rho = 0$. In this approximation it is possible to show that the electric field (and also the magnetic field) must satisfy the wave equation [18]:

$$\Delta\vec{E} - \varepsilon\mu\frac{\partial^2\vec{E}}{\partial t^2} = 0 \tag{8}$$

This is a standard equation of wave motion which shows the existence of electromagnetic [19] waves propagating with a velocity:

$$v = \frac{1}{\sqrt{\varepsilon\mu}} \tag{9}$$

If the medium is the vacuum, then the velocity is the speed of light:

$$c = \frac{1}{\sqrt{\varepsilon_0\mu_0}} \tag{10}$$

where ε_0 and μ_0 denote the permittivity and the permeability of vacuum, respectively.

One of the possible solutions of the wave equation (8), which is often used for describing light, is a plane wave. It can be expressed in complex notation (the magnetic field analogically):

$$\vec{E}(\vec{r}, t) = \vec{E}_0(\vec{r})e^{-i(\omega t - \vec{k}\cdot\vec{r} + \varphi)} \tag{11}$$

where $\vec{E}_0(\vec{r})$ is the complex amplitude (it can be generally a function of space) ω is the angular frequency, $\vec{k}$ is the wave vector and φ is the initial phase. In addition, the wave vector and the angular frequency are not independent; they must adhere to the dispersion relation:

$$k = |\vec{k}| = \frac{\omega}{c} \tag{12}$$

2.1.2. Index of refraction and absorption

The index of refraction *n* of an optical medium is a dimensionless number that describes how light, or an electromagnetic wave, propagates through that medium. It is defined as [18]:

$$n = \frac{c}{v} \tag{13}$$

where *c* is the speed of light in vacuum and *v* is the phase velocity of light in the medium. It also plays an important role when describing propagation of light from one medium into another medium (reflection and refraction). For isotropic, homogeneous, non-conductive medium (dielectric) without free charge is the index of refraction a real number. Then, substituting (9) and (10) into (13) we can express the index of refraction in terms of the material properties:

$$n = \sqrt{\varepsilon_r \mu_r} \tag{14}$$

We used common notation $\varepsilon = \varepsilon_0 \varepsilon_r$ and $\mu = \mu_0 \mu_r$, where ε_r denotes the relative permittivity and μ_r the relative permeability.

On the other hand, for absorbing (e.g. conducting) medium *n* is a complex number. Then we define the complex index of refraction and the complex wave vector as follows:

$$\hat{n} = n + i\kappa \tag{15}$$

$$\hat{k} = (n + i\kappa)\frac{\omega}{c} = k + i\kappa\frac{\omega}{c} \tag{16}$$

where *n* is real part of index of refraction, κ (a real number) is called the extinction coefficient, which measures the amount of absorbed light when propagating through material and *i* denotes an imaginary unit. When

approximating light by monochromatic harmonic plane wave, it is possible to show that there is an exponential absorption along the axis in which light is propagating [18]:

$$\vec{E}(\vec{r},t) = \vec{E}_0(\vec{r})\mathrm{e}^{-i(\omega t - k\vec{r}.\vec{s})}\mathrm{e}^{-\frac{\omega}{c}\kappa\vec{r}.\vec{s}} \tag{17}$$

Here $\vec{s}$ is a real unit vector specifying the direction of light propagation.
To determine the complex index of refraction, we need a microscopic model that describes interaction of light with matter.

For conducting materials (e.g. metals), it is possible to derive extinction coefficient from Maxwell's equations by defining effective relative permittivity (a complex number) as [18]:

$$\widehat{\varepsilon_r} = \varepsilon_r + i\frac{\sigma}{\omega\varepsilon_0} \tag{18}$$

In case of a conducting material, we have to use the effective relative permittivity which results in the complex index of refraction:

$$\hat{n} = \sqrt{\widehat{\varepsilon_r}\mu_r} \tag{19}$$

Substituting (18) into (19) and using the definition (15) we can determine the extinction coefficient [18]:

$$n^2 = \frac{1}{2}\left(\sqrt{\mu_r^2\varepsilon_r^2 + \frac{\mu_r^2\sigma^2}{\omega^2\varepsilon_0^2}} + \mu_r\varepsilon_r\right) \tag{20}$$

$$\kappa^2 = \frac{1}{2}\left(\sqrt{\mu_r^2\varepsilon_r^2 + \frac{\mu_r^2\sigma^2}{\omega^2\varepsilon_0^2}} - \mu_r\varepsilon_r\right) \tag{21}$$

In metals, on account of their very high conductivity, an electromagnetic wave is attenuated on microscopic scale and they are practically opaque. Strong absorption is accompanied by a high reflectivity, so that metallic surfaces act as excellent mirrors.

2.1.3. Phenomenological description

Solid-state physics shows how macroscopic properties of solid materials can be explained by atomic-scale properties. One of the successful theories (and most common) is the band theory. It shows that atoms in a large, periodic lattice (crystal structure) cannot be treated separately, but we have to incorporate their mutual interaction, which can be described by an effective periodic potential. Then instead of discrete energies as in the case of electrons in atoms, the available energy states for electrons form energy bands. In insulators, the electrons in valence band are separated by a large gap (called band gap) from the conduction band. In conductors, the valence band overlaps the conduction bands. In semiconductors, the band gap is small enough that under certain conditions electrons can be excited into the conduction band. Therefore conductivity of a semiconductor depends on internal and external parameters, such as temperature, doping, or even incoming electromagnetic radiation.

We have shown in chapter 2.1.2 that the complex refractive index can describe propagation of light, its velocity and absorption in a material. Now we will study the properties of the refractive index with the help of microscopic models. We will use two classical approaches, which exclude quantum effects: Lorentz's model for dielectric materials and Drude's model for conductors and semi-conductors.

In Lorentz's model are atoms (or molecules) of a material treated as classical dipole oscillators. We assume that a nucleus and an electron in an atom are elastically bound. If there is no external field acting on the atom, the electric dipole is zero. However an external electric field forces oscillation of the electron in the frequency of light. This model uses Newton's equation of motion to describe an electron displacement from equilibrium within an atom (since the mass of the nucleus is much bigger, its motion is negligible). The electric field pulls on the electron with electric force $q\vec{E}$, drag force $m\gamma\dot{\vec{x}}$ opposes the electron motion and accounts for absorption of energy and finally, restoring force $k_{hook}\vec{x}$ (Hooke's law) accounts for the fact that electron is bound to the nucleus [19]:

$$m\ddot{\vec{x}} = q\vec{E} - m\gamma\dot{\vec{x}} - k_{hook}\vec{x} \tag{22}$$

This equation is solved for a harmonic electromagnetic wave which wavelength is much longer than the size of the atom. Thus the electric field of light acting on the electron is constant in space where electron oscillates, and it is only a function of time. It is possible to derive an expression for the complex refractive index [19]:

$$(n + i\kappa)^2 = 1 + \frac{\omega_p^2}{\omega_0^2 - i\omega\gamma - \omega^2} \tag{23}$$

Here ω is the frequency of light, ω_0 is the natural oscillation frequency associated with the electron mass and the 'spring constant' k_{hook}, ω_p is the plasma frequency (corresponds to natural oscillation frequency of free ions in plasma), and γ dumping coefficient used in (22). A graph of n and κ are given in Figure 1, with the use of Kramers-Kronig relations [20]. These are mathematical relations, connecting the real and imaginary parts of a complex function. Therefore they are often used to calculate the real part from the imaginary part (or vice versa) in stable physical systems.

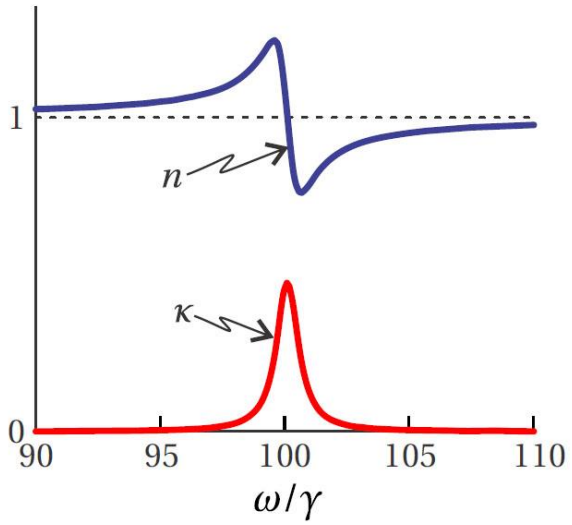

Figure 1: Real and imaginary parts of the index for a single Lorentz oscillator dielectric with $\omega_p = 10\gamma$ and $\omega_0 = 100\gamma$. *Source [19].*

If the frequency of light is near the natural frequency of the oscillator $\omega \approx \omega_0$, exchange of energy occurs and the light is absorbed. If these

frequencies differ, absorption is negligible and the atoms oscillate at the frequency of light but with a certain phase shift.

In Drude's model for conducting medium, the outer electrons of atoms are free to move without being tethered to any particular atom. However, the electrons are still subject to a damping force due to collisions that remove energy and give rise to absorption. As it turns out, we can obtain a simple formula for the refractive index of a conductor from the Lorentz model by removing the restoring force that binds electrons to their atom (derivation is provided in [19]). That is equal to setting $\omega = \omega_0$, which gives

$$(n + i\kappa)^2 = 1 - \frac{\omega_p^2}{i\omega\gamma + \omega^2} \tag{24}$$

A graph of n and κ is given in Figure 2.

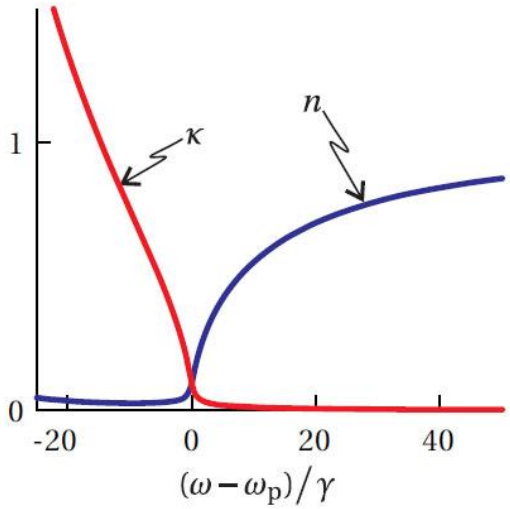

Figure 2: Real and imaginary parts of the refractive index for conductor with $\omega_p = 50\gamma$. *Source [19].*

If the damping coefficient is negligible compared with the frequency of light, (24) reduces to:

$$(n + i\kappa)^2 = 1 - \frac{\omega_p^2}{\omega^2} \tag{25}$$

Now we can see that for frequencies $\omega > \omega_p$, the refractive index is a real number and the material is transparent. However if $\omega < \omega_p$, the refractive index is a complex number and absorption occurs. In next chapters we will

see, that absorption is accompanied by high reflectivity, so that metallic surfaces act as excellent mirrors.

2.2. Polarization of light

Polarization is a property of light that describes the orientation of electric field $\vec{E}$ and its evolution in time and space. It should be noted that magnetic field oscillates as well and it is only a convention to describe polarization by electric field. The main reason for this convention is that the magnetic field usually has negligible effect on materials (with comparison to the electric field).

Polarization can have a huge impact on how the light propagates (e.g. in anisotropic media). To describe polarization, we assume a plane monochromatic harmonic wave which propagates in homogenous isotropic non-conductive medium without charge density (direction of propagation is along *z*-axis):

$$E_x = a_x \cos\left[\omega\left(t - \frac{z}{v}\right) + \varphi_x\right] \tag{26}$$

$$E_y = a_y \cos\left[\omega\left(t - \frac{z}{v}\right) + \varphi_y\right] \tag{27}$$

where E_x, E_y are *x* and *y* components of the electric field, a_x and a_y are amplitudes, φ_x and φ_y are corresponding phases. It can be shown from Maxwell's relation that the electric field $\vec{E}$ can generally oscillate in an elliptic shape [18]:

$$\left(\frac{E_x}{a_x}\right)^2 - 2\frac{E_x E_y}{a_x a_y}\cos\varphi + \left(\frac{E_y}{a_y}\right)^2 = \sin^2\varphi \tag{28}$$

where $\varphi = \varphi_y - \varphi_x$. The polarization ellipse is shown in Figure 1.

To fully describe polarization 4 parameters are needed. However, in most cases we only need 3 parameters, because the last one sets the initial phase (which is usually not of concern). There are many combinations of

parameters that define the ellipse, for example combination of a_x, a_y and φ according to (12). Figure 3 shows the polarization ellipse.

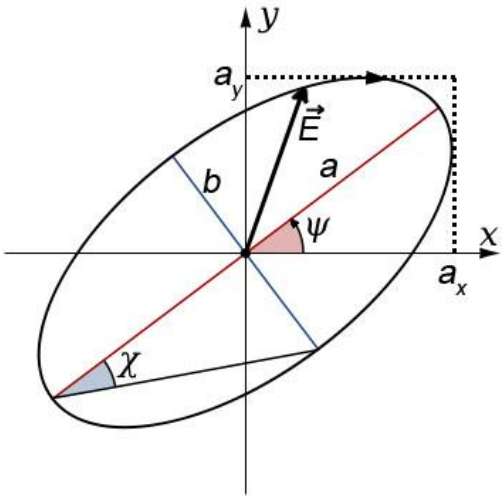

Figure 3: Polarization ellipse and various possible parameters.

There are special cases of elliptical polarization: linearly and circularly polarized light. It should be noted that in different conventions (e.g. direction of propagation, signs of phases etc.) are the definitions different, but must represent same physical reality. Linear polarization occurs if:

a) One of the components of the electric field is zero (either $a_x = 0$ or $a_y = 0$)
b) Arbitrary amplitudes but phase difference $\varphi = 0$ or $\varphi = \pi$.

Circular polarization occurs if amplitudes are equal $a_x = a_y$ and at the same time $\varphi = \pm \pi/2$. Circular polarization may be referred to as right-handed (clockwise) or left-handed (anti-clockwise) depending on the direction in which the electric field rotates. If we look from the point of view of the receiver (as in Figure 1, we are looking against the direction of propagation of light) at a constant point z, then if:

a) $\varphi = + \pi/2$: electric field $\vec{E}$ rotates in clockwise direction, thus it is called right-handed (clockwise) circular polarization.
b) $\varphi = - \pi/2$: electric field $\vec{E}$ rotates in anti-clockwise direction, thus it is called left-handed (anti-clockwise) circular polarization.

2.2.1. Jones vectors and matrices

Fully polarized light can be described using the Jones calculus. Polarized light is represented by a Jones vector, and linear optical elements are represented by Jones matrices. When light crosses an optical element, the resulting polarization of the emerging light is found by taking the product of the Jones matrix of the optical element and the Jones vector of the incident light. We will use an electromagnetic wave in the form as in the previous chapter:

$$\vec{E} = E_x\vec{x} + E_y\vec{y} \tag{29}$$

Here $\vec{x}$ and $\vec{y}$ are unit vectors along *x* and *y* axis, E_x and E_y are defined in (26) and (27) but using complex formalism:

$$E_x = a_x \mathrm{e}^{i(\omega t - kz + \varphi_x)} = A_x \mathrm{e}^{i(\omega t - kz)} \tag{30}$$

$$E_y = a_y \mathrm{e}^{i(\omega t - kz + \varphi_y)} = A_y \mathrm{e}^{i(\omega t - kz)} \tag{31}$$

Complex amplitudes A_x and A_y carry information also about the initial phase. Jones vector of polarized light is then defined:

$$\vec{\mathrm{J}} = \begin{pmatrix} A_x \\ A_y \end{pmatrix} \tag{32}$$

This vector carries complete information about the polarization state.

An optical element is represented by 2x2 Matrix *M*. Then we can describe the resulting polarization state as (subscripts out and int denote outcoming and incoming light):

$$\vec{\mathrm{J}}_{out} = M\vec{J}_{in} \tag{33}$$

If we put more than one optical element, then equation (36) transforms into:

$$\vec{\mathrm{J}}_{out} = M_n \ldots M_2 M_1 \vec{J}_{in} \tag{34}$$

where M_n denotes the matrix of the n-th optical element that light goes through.

2.2.2. Transmission and reflection: Fresnel equations

Behaviour of light when moving between media of differing indices of refraction is described by Fresnel equations (together with Snell's law and law of reflection). More precisely, these equations describe amplitudes of the transmitted, the reflected wave and also their phase shifts. To write these equations, we have to set directions of propagation and polarization. We choose convention as in Figure 4.

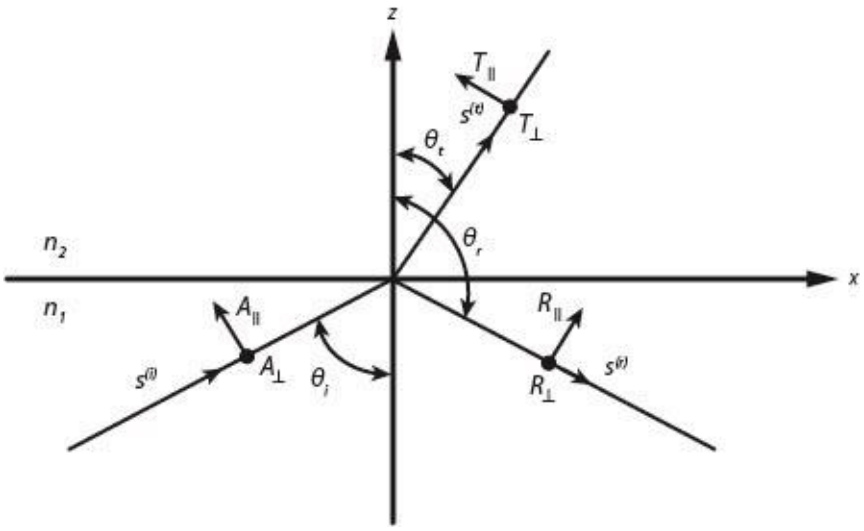

Figure 4: Specifications for transmission and reflection.

Then Fresnel formulae are [18]:

$$t_\parallel = \frac{2n_1 \cos\theta_i}{n_2 \cos\theta_i + n_1 \cos\theta_t} A_\parallel \tag{35}$$

$$t_\perp = \frac{2n_1 \cos\theta_i}{n_1 \cos\theta_i + n_2 \cos\theta_t} A_\perp \tag{36}$$

$$r_\parallel = \frac{n_2 \cos\theta_i - n_1 \cos\theta_t}{n_2 \cos\theta_i + n_1 \cos\theta_t} A_\parallel \tag{37}$$

$$r_{\perp} = \frac{n_1 \cos\theta_i - n_2 \cos\theta_t}{n_1 \cos\theta_i + n_2 \cos\theta_t} A_{\perp} \tag{38}$$

Here *a*, *r*, *t*, denote complex amplitudes of the electric vector (as introduced in previous chapter) of incoming, reflected, and transmitted wave respectively. Subscripts $\perp$ and $\parallel$ indicate polarization perpendicular and parallel to the plane of incidence, respectively. Plane of incidence is a plane defined by the wave vector of the incoming light and the normal to the boundary between materials.

3. Experimental Methods

3.1. Spectroscopic ellipsometry

Ellipsometry is an optical technique for investigating the dielectric properties (e.g. complex refractive index) of thin films. Ellipsometry can be used to characterize composition, roughness, thickness and other material properties associated with a change in optical response. Ellipsometry can yield information about layers that are thinner than the wavelength of the probing light, ranging from a few angstroms to several micrometres. As an optical technique, it is non-destructive and contactless. However, the one weakness of ellipsometry is the need to model the acquired data. The name “ellipsometry” comes from the fact that elliptical polarization of light is used. The term “spectroscopic” relates to the fact that the information gained is a function of the light’s wavelength or energy.

3.1.1. Basic principles

Ellipsometry is primarily interested in how parallel and perpendicular components of electric field change upon reflection or transmission in relation to each other. A known polarization is reflected or transmitted from the sample and the output polarization is measured. The change in polarization is the ellipsometry measurement, defined as a complex ratio of total reflection coefficients [21]:

$$\rho = \frac{R_{\parallel}}{R_{\perp}} \tag{39}$$

Total reflection coefficients $R_{\parallel}$ and $R_{\perp}$ are defined as the ratio of the amplitude of the resultant reflected wave to the amplitude of the incident wave for the parallel and perpendicular components with regard to the plane of the incidence (as defined in previous chapter).

We denote the phase difference between the parallel component and the perpendicular component of the incoming wave as φ_1. Similarly, we

denote phase difference of the outgoing wave (after interaction with matter) as φ_2. Then we define the parameter called delta (abbreviated "*Del*") as

$$\Delta = \varphi_1 - \varphi_2 \tag{40}$$

Del is then the change in phase difference that occurs upon reflection and its value can be from zero to 360 degree.

Without regard to the phase, the amplitude of both perpendicular and parallel components may change upon reflection. We define a quantity called "*Psi*" as:

$$\tan \Psi = \frac{|R_{\parallel}|}{|R_{\perp}|} \tag{41}$$

Psi is then the angle whose tangent is the ratio of the magnitudes of the total reflection coefficients, and it can vary from zero to 90 degree.

The equation (39) can be expressed as:

$$\rho = \tan \Psi \, \mathrm{e}^{i\Delta} \tag{42}$$

and it is called the fundamental equation of ellipsometry.

"Pseudo" optical constants can be obtained from ρ:

$$\langle \hat{\varepsilon} \rangle = \sin^2(\phi) \left[1 + \tan^2(\phi) \left(\frac{1-\rho}{1+\rho} \right)^2 \right] \tag{43}$$

where ϕ is the angle between the incoming light and the normal of the surface. They are called "pseudo", because this equation assumes that there is a bulk material with ideally smooth surface and no additional layers, which is impossible in reality. Therefore data analysis and models are required.

3.1.2. Experimental setup

Electromagnetic radiation is emitted by a light source and linearly polarized by a polarizer. It can pass through some compensators (quarter wave plate) and falls onto the sample. After reflection the radiation passes

through a second polarizer, which is called an analyser, and goes straight into the detector. This setup is depicted in Figure 5.

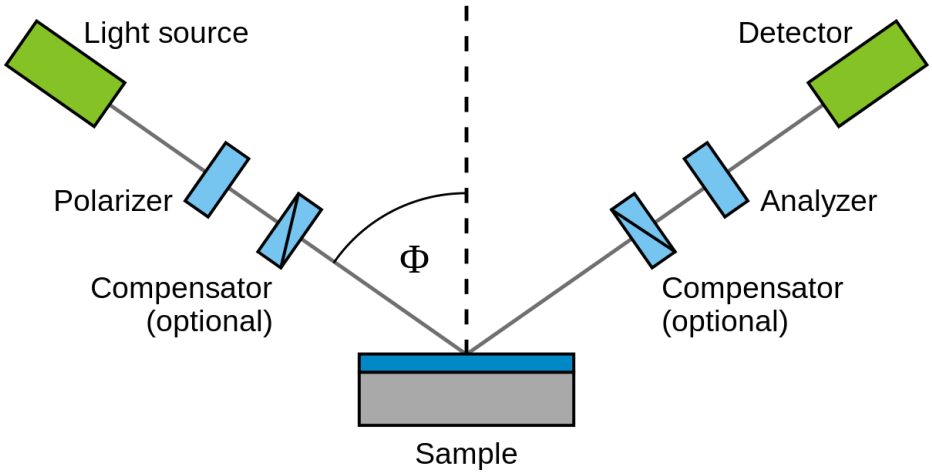

Figure 5: Conceptual setup of ellipsometer.

The first requirement is to have monochromatic polarized light. As in Figure 5, laser beam passes through a polarizer. After the reflection on the surface, the light would come out, in general, elliptically polarized. Linearly polarized light is much simpler to analyse since we can use another polarizer (called analyser) to determine the null and hence the angle of polarization. To change the light from elliptical into linear polarization we use the quarter wave plate (QWP), which needs to be aligned appropriately. The angles of the QWP and the analyser required to extinguish the light provide information about the phase difference and attenuation caused the reflection and hence allow us to calculate *Del* and *Psi*.

We use Various Angle Spectroscopic Ellipsometer (VASE), which measures one material at more angles. This gives better accuracy, since the pseudo optical constants depend on this angle (e.g. equation (43)).

A material is considered to be a substrate if we do not have to deal with any lower boundaries, typically because light is totally absorbed in the substrate. A film, on the other hand, will be a material transparent enough that the underlying layer must be taken into account.

Thickness of a thin film is determined by interference between light reflecting from the surface and light traveling through the film.

3.1.3. Data analysis

To determine material properties, we always need an assumed model. In the case of a bulk material, there is only a single reflection and it is straightforward to calculate optical constants from *Del* and *Psi*. However, in any bulk material, there is typically a surface oxide or roughness, which has to be included in the model. The most common procedure used to deduce material properties follows the flow chart in Fig 12. Regression analysis is required because an exact equation cannot be written.

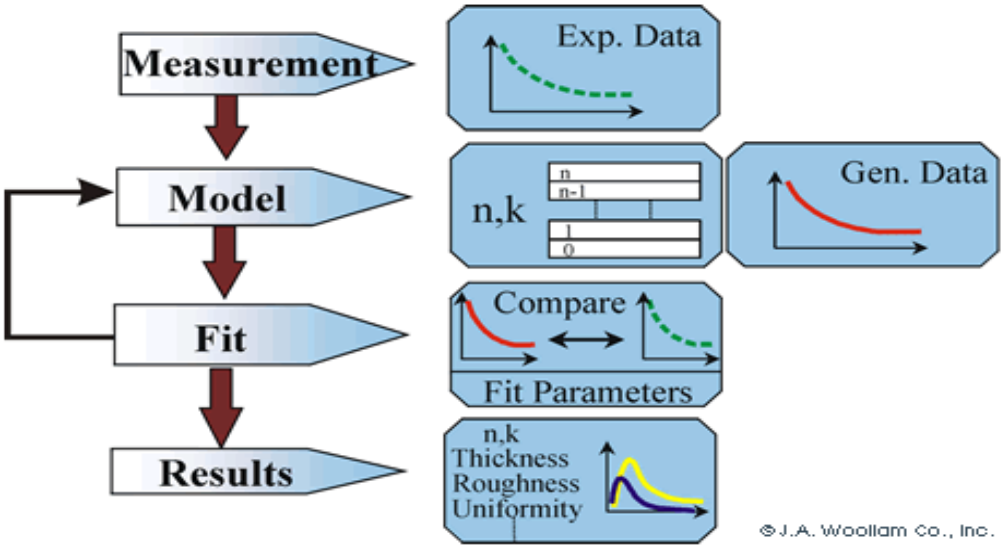

Figure 6: Flowchart for ellipsometry data analysis. *Source [22].*

After a sample is measured, a model is constructed to describe the sample. The model is used to calculate the predicted response from Fresnel's equations. These calculated data are compared to experimental data. Any fit parameter of the model can then be varied to improve the match between the experiment and calculation. Mean Squared Error (MSE) is used to quantify the difference between curves, or "goodness" of fit. The unknown parameters are allowed to vary until minimum MSE is reached.

It should be noted that assuming the instrument is operating properly, the quantities *Del* and *Psi* which are measured are correct. Whether the calculated sample parameters such as thickness and index of refraction are correct depend on whether the model assumed is correct.

3.1.4. Models for CdTe

VASE ellipsometer used was purchased from commercial company J.A. Woollam Co. Inc., which comes with software for data analysis CompleteEASE. This software contains predefined models for common materials, including CdTe and CdTe oxide. The CdTe material is parameterized by Lorentz oscillators and the CdTe oxide is parameterized with the Cauchy equation.

An optimal approach for finding the best model is to start with the simplest model. If the fit is insufficient, what means that the MSE is too huge, we have to use a different, more complex model. We repeat this process until MSE is low enough. According to CompleteEASE manual, an ideal model fit should have an MSE of ≈1, however the best model fits for more complex samples may exhibit much larger MSE's (≈10) and still be considered acceptable. Therefore, when evaluating a model not only the value of the MSE is necessary, but also whether fit parameters are physically possible.

First used model was CdTe substrate and simple CdTe oxide layer (Figure 7a). Since this was insufficient, effective medium approximation (EMA) and surface roughness were included (Figure 7b). Surface roughness substitutes a non-uniform surface layer with material peaks and trenches by an average value, which described how thickness varies throughout the surface. In EMA are the optical constants of the consisting material (CdTe and oxide) mixed in the ratio 0-100%. This model enabled estimation of thickness of surface layer with MSE less than 5.

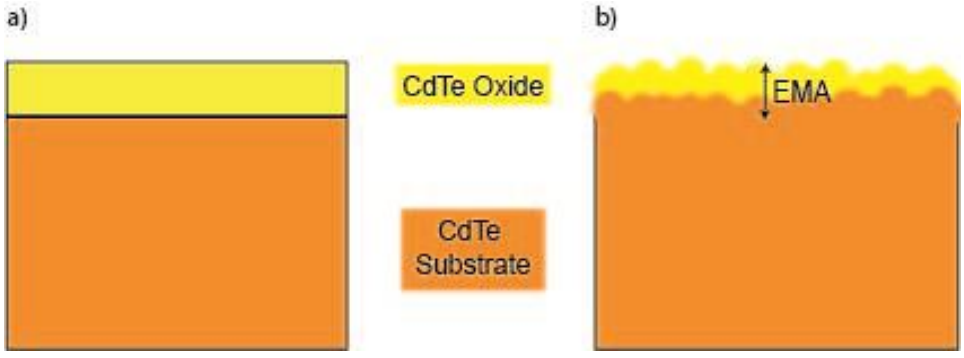

Figure 7: a) Ideally smooth surfaces, b) EMA model with surface roughness

3.2. Volt-Ampere characteristic

The dependence of dark electric (leakage) current on the applied bias (I-V characteristics) is measured using a simple 2-probe measurement. Keithley SourceMeter 2410 serves as bias source. The contacted CdZnTe sample is inserted into a voltage divider circuit with a known serial resistor. The resistor in our measurement has the resistance value of 100 MΩ. It is a commercial resistor with the resistance accuracy of 0.1 %. The electric current of the sample is measured with Keithley Electrometer 6517a via the voltage readout on the serial resistor and then recalculated to the electric current. Our setup is fully automatized with computer control. The sample was biased in the range of -700 to +700 V (with a step of 50 V), as these are typical bias values for CdTe detectors. It should be noted that the dimensions of our samples do not meet the standards used for radiation detectors. Our samples are utilized for ellipsometry measurement and have rather small contacts and large lateral sides. This results in a relatively lower measured current than on detectors. However, we employ the I-V characteristics measurement to evaluate the relative change of the current in dependence on time and to correlate it with oxide and surface layer thicknesses evolution measured with ellipsometry.

The samples were kept in dark environment for one hour prior to the I-V measurement. After biasing, a time delay of 5 minutes between each step was set for the current measurement to avoid sample relaxation during measurement etc. An average of at least 20 readouts from the electrometer was used to determine the value of electric current.

4. CdZnTe Samples

CdZnTe material used was a commercially available single crystal with diameters 20×20×5 mm^3. The material resistivity measured using the contactless mapping method was of the order ~10^{10} Ω·cm and is depicted in Figure 8. This material was cut into 8 smaller samples of size 7×6×2mm^3. We label them as A1, A2, B1, B2, C1, C2, D1 and D2. After cutting with a diamond saw, the samples were mechanically polished using 1 μm alumina (Al_2O_3) abrasive, which was taken as the initial state before contacting and surface preparation. Largest surface area was used for ellipsometry.

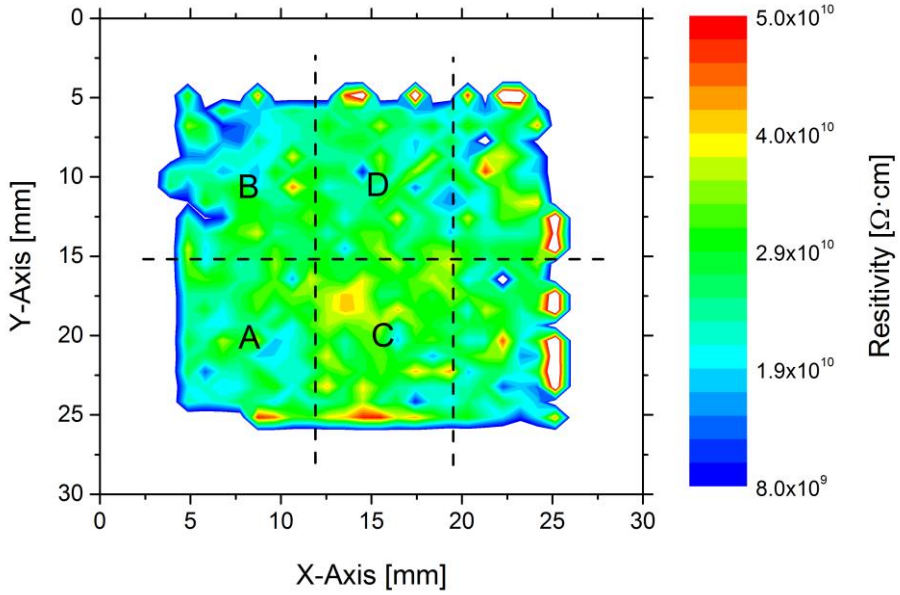

Figure 8: CdZnTe material resistivity.

4.1. Preparation of the samples

The notation of surfaces of the samples is illustrated in Figure 9. Surfaces 1, 2 were contacted for electrical measurements. The surfaces 1-4 were covered with polystyrene which is inert to chemical etching using bromine solutions; the surfaces 5, 6 were chemically prepared (etching, passivation). Methodical procedure for samples is following:

1. Mechanical polishing and chemical etching with 0.1% Br-MeOH for 60s to remove the damaged surface layer.

2. Masking samples for electrical contacts.
    a. Covering of surfaces 3-6 by photoresist.
    b. Preparation of golden contacts on surfaces 1-2.
    c. Wire contacting using colloid silver solution.
3. Covering contact surfaces 1-2 with polystyrene.
4. Covering side surfaces 3-4 with polystyrene.
5. Chemical etching of surfaces 5 and 6 (oriented plane <111>) in 1% Br-MeOH for 60s to remove surface roughness.
6. Immediate ellipsometry measurement (within several minutes).
7. Chemical etching of surfaces 5 and 6 (Br-MeOH 1% solution for 60 seconds) and immediate passivation in KOH or NH_4F. The passivation is skipped for the sample intended for the growth of native oxide.
8. Immediate ellipsometry measurement.
9. Long-time scale measurement (every week) using ellipsometry and volt-ampere characteristic.

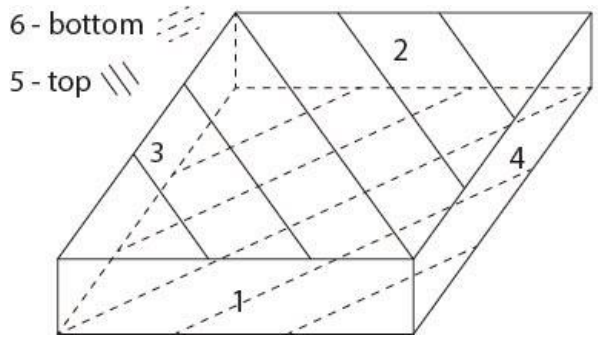

Figure 9: Sample surface notation.

4.2. Native oxides and passivation

The samples were used to study different surface layers. After the preparation of samples, every sample was passivated with different method. The sample A1 was used to study native oxides; the A2 and C1 were treated with KOH solution for 2 minutes, B2 with KOH solution for 5 minutes and C2 with NH_4F solution for 2 minutes. Sample B1 was damaged, sample D1 was not used and sample D2 was used for the XPS measurement.

5. Results

Every sample was prepared as described in chapter 4.1. After preparation the samples were measured on the VASE ellipsometer with configuration as follows: reflection mode with four incident angles Φ = 55°, 60° and 65° degree, acquisition time 60 seconds, photon energy from 1.24 eV to 4.0 eV. The incident beam and the position of the sample were calibrated before every measurement for better accuracy. The incident light diameter was 4mm, what was enough to cover most of the surface; therefore measured information was averaged over the whole surface. After ellipsometric measurement the contacts of the samples were glued with conductive silver paste on special plate and volt-ampere (I-V) characteristic was measured. This process was repeated every week for a period of up to five months.

Because of the non-uniformity of the surface and the layer interface, we evaluate the effective thickness of the surface layer as thickness of the EMA layer + 0.5 × roughness of the EMA layer. In the EMA layer, which is coupled to the substrate material, the parameters of CdTe are the same as of the substrate.

Ellipsometry measurements were evaluated using “Multi Sample Analysis” function in CompleteEASE software, where the optical parameters of the substrate and the EMA layer must remain constant for the all data sets corresponding to one sample. Only the ratio, the thickness, the roughness of the EMA layer and the angular spread can change individually in each measurement. Phrase “Multi Sample Analysis” could be confusing, since we use data sets of one sample at different times; therefore phrase “Multiple Datasets Analysis” is used.

The accuracy of measuring ellipsometric parameters *Del* and *Psi* is much better when compared to errors resulting from fitting parameters of a model. Therefore the errors in estimation of thickness and roughness (and other fit parameters) are only dependent on the MSE of a model.

5.1. Native oxides

5.1.1. Ellipsometry

Sample A1 was observed for about 5 months. Figure 10 illustrates the typical evolution of parameters *Psi* and *Del* over time after surface treatment. The significant decrease of *Del* is directly connected to the growth of native oxide.

The measured data were evaluated using the model described in chapter 4.1.3. The fit of all measured data, using multiple datasets analysis, was successful with the MSE of about 1.25. That corresponds to an almost ideal model. The error in thickness and roughness was ± 0.2 nm.

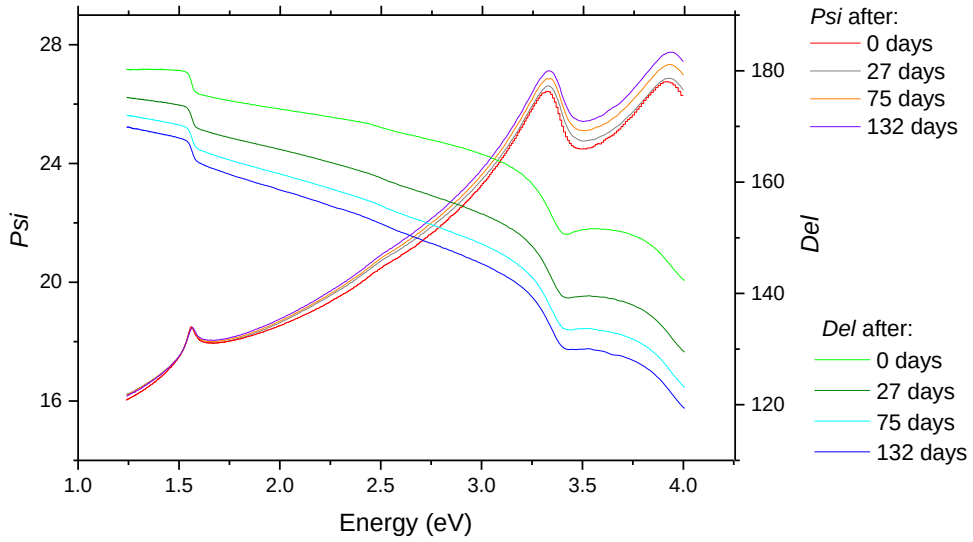

Figure 10: Evolution of ellipsometry parameters of sample A1 up to 5 months.

The thickness and roughness time evolution of the EMA layer is depicted in Figure 11. The initial value of the thickness and the roughness, after the surface treatment, was very close to zero. A semi-saturation of the oxide growth was observed after approximately 7 days with the thickness of about 4 nm. Then the increase in roughness was much larger when compared to the thickness, which changed negligibly during the next five month period. This could be eventually attributed to the casual use of the sample, when being transported, prepared for measurements, etc. However, since the roughness increases almost linearly over time (after the semi-saturation), the reason is more likely to be mechanical stress and lattice

mismatch of the surface layer. It should be noted that the evaluated roughness is only a result of ellipsometric measurement, which does not measure it directly. In CompleteEASE, roughness is calculated by a mix of the top layer of the model and air in 50%-50% ratio. Therefore it represents the average roughness of the whole surface and does not have to correspond to what would be measured using different methods (e.g. AFM, optical interferometry). That is subject for further research.

The time evolution of the effective thickness is depicted in Figure 12, where the semi-saturation period can be seen as well. After the semi-saturation, the increase in the effective thickness stabilized and was almost linearly dependent on time.

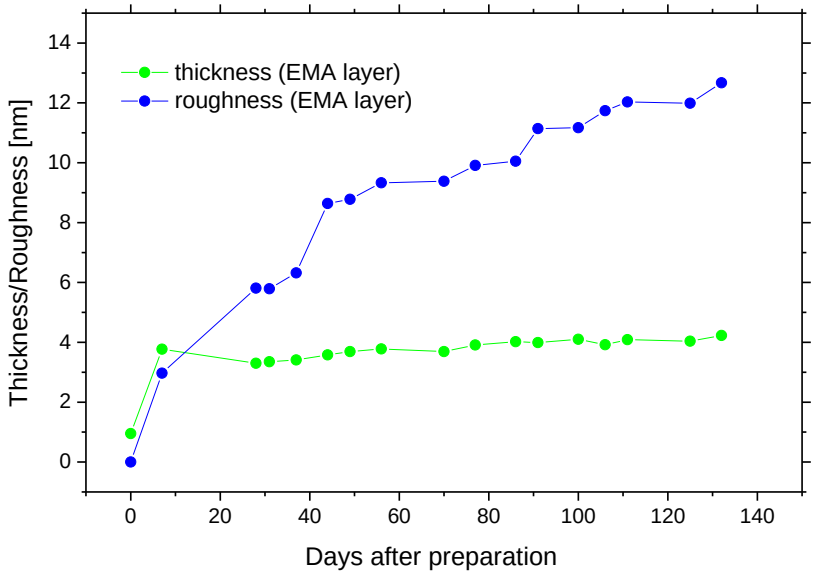

Figure 11: Time evolution of the thickness and roughness of the EMA layer of sample A1s over 5 months.

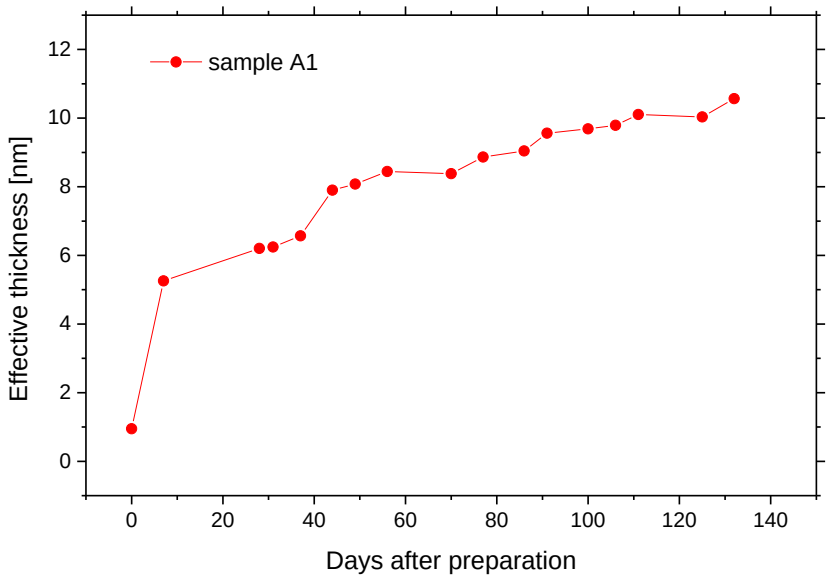

Figure 12: Time evolution of the effective thickness of sample A1 over 5 months.

Measured I-V characteristics are depicted in Figure 13. For illustration purposes, the current measured at 400 V bias is depicted in Figure 14 as it evolves in time. After surface preparation, there is a slight decrease in the current. However, after 7 days the current increased to about 27 nA (at 400 V). The reason is most likely the rapid oxide growth, observed in ellipsometric measurements, which could alter the surface structure or chemistry resulting in increased currents. Subsequently, the current decreased and stabilized at about 4 nA.

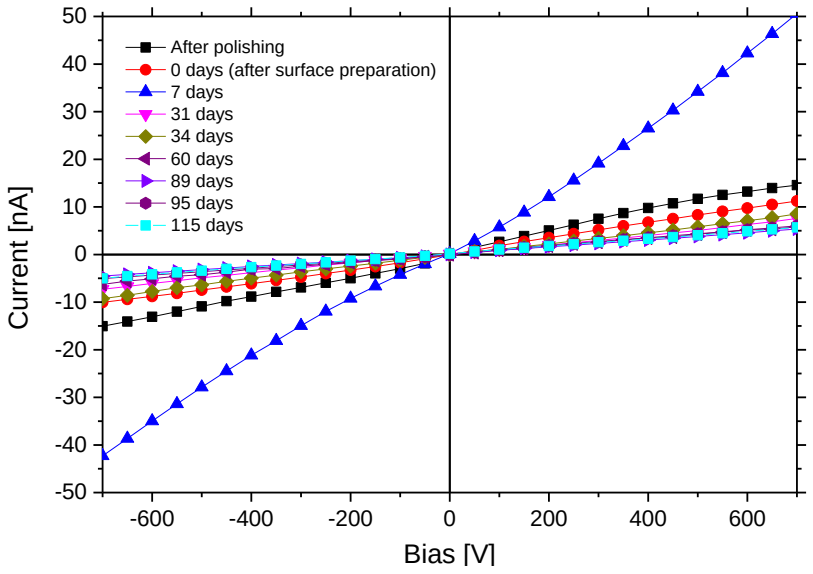

Figure 13: I-V characteristics evolution of sample A1 over 5 months.

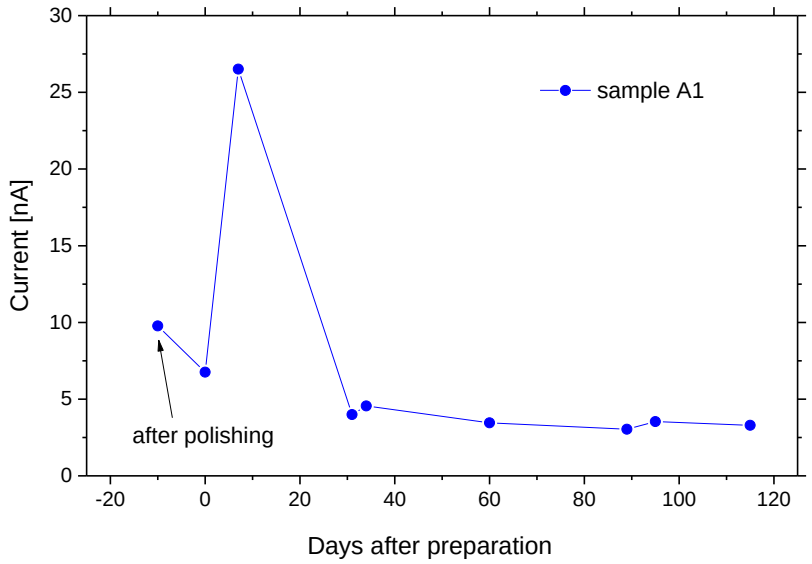

Figure 14: Time evolution of the leakage current at 400 V bias. Point at -10 days represents measurement after mechanical polishing (before surface preparation).

The parameters of the CdTe substrate and CdTe oxide, which have been fitted, describe the complex index of refraction as a function of the wavelength (or energy) of light. They are depicted in Figure 15 (CdTe substrate) and Figure 16 (CdTe oxide). As we will see in the next chapters, for samples that have been passivated there is a need for a different model. However, the parameters of the substrate and the oxide should not vary; therefore they are used in models for other samples.

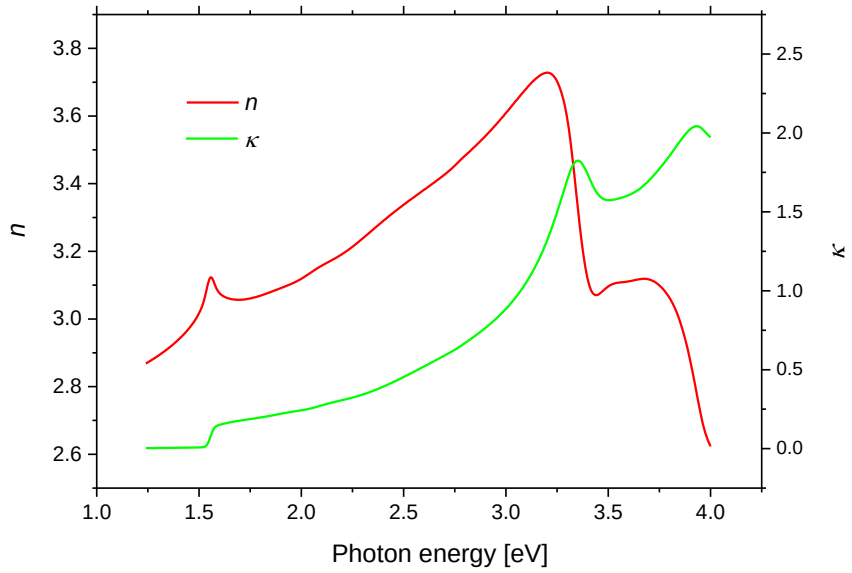

Figure 15: Real part (n) and imaginary part (extinction coefficient κ) of the complex refractive index of the CdTe substrate as a function of photon energy (wavelength of light).

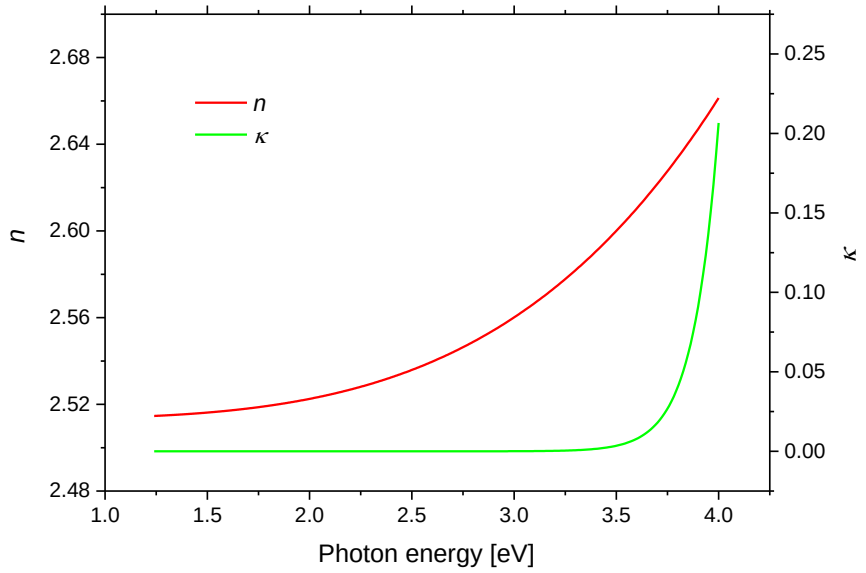

Figure 16: Real part (*n*) and imaginary part (extinction coefficient *κ*) of the complex refractive index of the CdTe oxide substrate as a function of photon energy (wavelength of light).

5.1.2. XPS measurements

To confirm that an oxide layer is grown on the sample surface after chemical etching, we studied sample D2 with x-ray photoelectron spectroscopy (XPS). XPS is a non-destructive investigation method, sensitive to surface changes of the studied sample. The sample is irradiated with a beam of x-rays. The radiation is scattered in the range of 0 – 20 nm of the material. In this depth, electrons are excited and escape their bound atom states and the material altogether. The amount of escaped (scattered) electrons and their kinetic energy is measured. Element composition and atomic ratio is evaluated.

XPS measurement of sample D2 was taken three times, after mechanical polishing, 2 hours after chemical etching and 3 weeks after chemical etching. Sample D2 was prepared identically as sample A1. No cadmium bound oxide has been found in any measurement. However, the ration of elemental tellurium and oxide bound to tellurium changes in time after etching.

The Tellurium 3d XPS spectra are depicted in Figure 17. The evaluated atomic ratios are in Table 2.

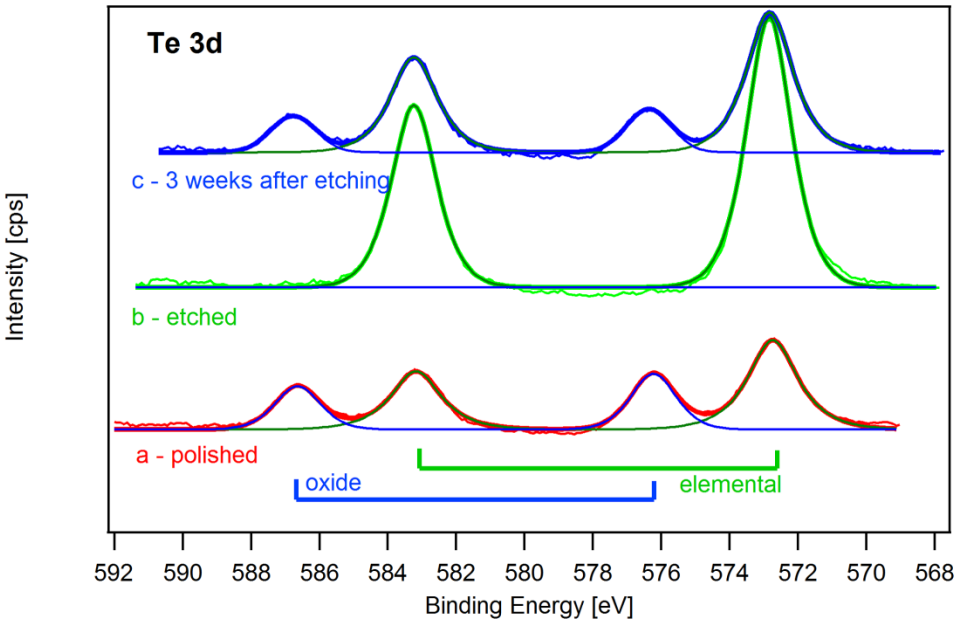

Figure 17: XPS spectra of the Te 3d measured after a - polishing, b - 2 hours after chemical etching and c - 3 weeks after chemical etching.

				stoichiometry ratio	**oxide ratio**
surface treatment	Te elemental	Te bound oxide	CdZn	∑Te/ ∑CdZn	Te bound oxide / Te elemental
polished	19.1	10.6	20.6	1.44	0.55
2 hour after etching	44.5	0.0	36.7	1.21	0.00
3 week after etching	28.0	8.3	28.0	1.30	0.30

Table 2: XPS data after polishing, 2 hours after chemical etching and 3 weeks after chemical etching

After sample polishing, we observed a great amount of oxide bound on tellurium found. As the sample is immersed into etching solution, all Te bound oxides are etched away and only Cd and Te is found on sample surface. However, the stoichiometry of the material changes slightly. Three weeks after sample etching, where the sample was held in ambient air at room temperature, the oxide ratio increases to 0.3. This indicates a growth of oxide bound to tellurium, supporting the results evaluated from ellipsometry measurements.

5.2. KOH passivation (2 minutes treatment)

Sample A2 was used to study influence of KOH passivation and was observed for up to 5 months. Since the 2 minute KOH passivation showed good initial results, sample C1 was also used to compare the results. Therefore sample C1 was observed for a shorter period (up to 2 months).

The EMA model with the CdTe oxide, which was successful for sample A1, was not sufficient for the KOH passivated surface layer. Therefore, a different model had to be incorporated. A new model, which better described the surface layer, consisted of the same EMA layer but with an additional constituent: elemental tellurium. Then the EMA layer is a mix of CdTe substrate, CdTe oxide and elemental tellurium in certain ratio between 0% and 100%.

The fit of all measured data was successful with the MSE of about 2.9 for sample A2 and 1.9 for sample C1 (lower MSE of C1 is due to a lower amount of measured data). That is not as good as in the case of sample A1; the passivation process alters the surface in a way that is not easily describable by ideal ellipsometric optical models. The error in thickness and roughness was ± 0.5 nm for sample A2 and ± 0.3 nm for sample A2.

The time evolution of the effective thickness of samples A2 and C1 is shown in Figure 18. The initial value (after passivation) of the effective thickness is larger than in sample A1, and it is followed by a nearly linear dependence on time. There is an absence of semi-saturation phase, with contrast to sample A1, even though the increase in the effective thickness is more significant during the first month than the next months. Noticeable difference between sample A2 and C1 is in the effective thickness, which is about 1-2 nm less for the C1 sample. This is slightly more than the estimated error. However, the surface and the surface preparation of every sample were not totally identical and therefore discrepancies can occur. The time evolution follows a similar pattern in both samples. The ratio of elemental tellurium in the EMA layer differs slightly; for sample A2 the ratio was in the range between 10% and 20%, and for sample C2 between 30% and 40%. That could be explained by a varying structure and chemistry of the surface even before the passivation.

Time evolution of the current measured at 400 V is depicted in Figure 19. In the case of sample A2, the current decreased to about 5 nA (compared to 50nA after polishing) immediately after the surface preparation and KOH passivation and was stable for the observed period. For sample C1, the current after surface treatment was higher (about 27 nA) but decreased after a week to values similar to those of sample A2. Measurement of the current after polishing for sample C1 was not possible due to technical reasons.

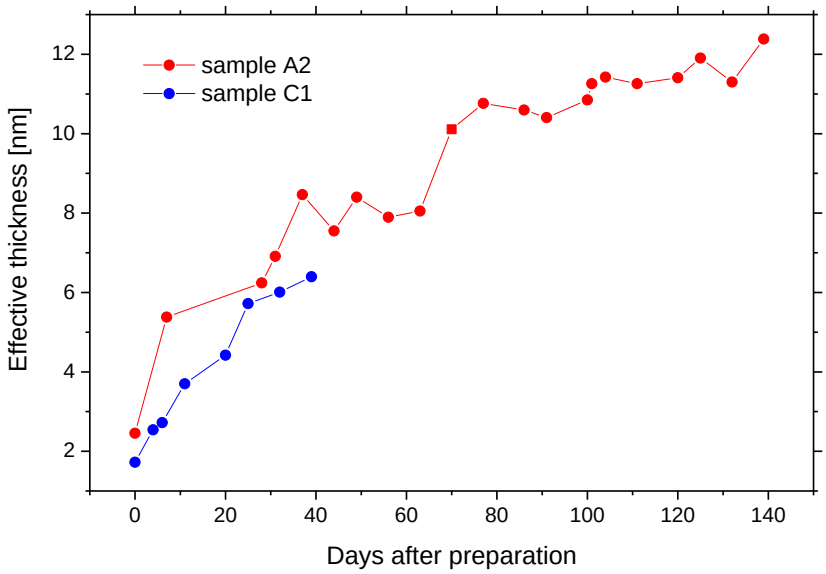

Figure 18: Time evolution of the effective thickness for up to 5 months of sample A2 and up to 2 months of sample C1.

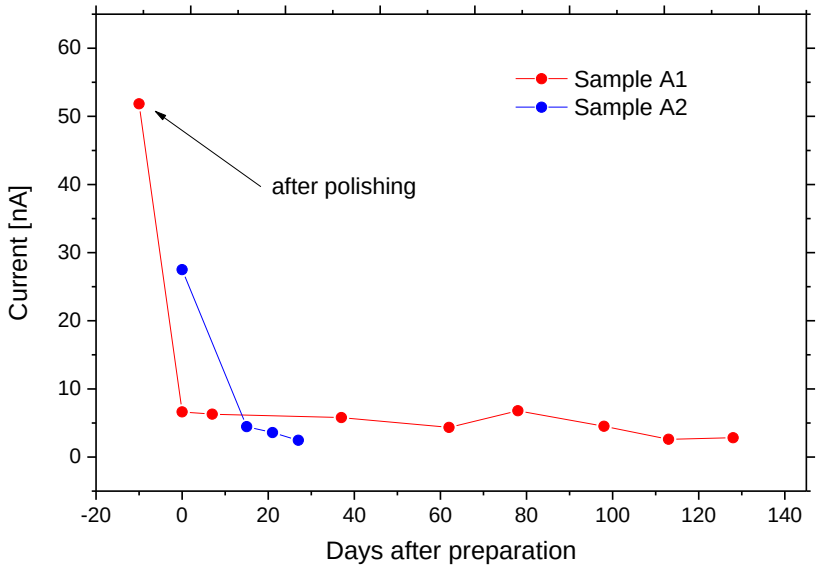

Figure 19: Time evolution of the leakage current at bias 400 V for up to 5 months of sample A2 and up to 2 months of sample C1.

5.3. KOH passivation (5 minutes treatment)

Sample B2, passivated by immersion into KOH solution for 5 minutes, was observed for up to 3 months. The ellipsometric model was the same as for samples A2 and C1. Fit of all measured data was successful with the MSE of 2.6. The error in thickness and roughness was ± 0.5 nm.

Time evolution of the effective thickness and current is depicted in Figure 20 and Figure 21, respectively. The surface layer growth is again linearly dependent on time; however the growth is significantly slower compared to samples A1, A2 and C1. The ratio of elemental tellurium drops from 40% after passivation to 15% after 3 months. The current gradually increases to about 45 nA after 2 months, which is much higher compared to previous samples. Five minute KOH treatment has destructive rather than passivating effects on the surface of CdTe. This might be due to atomic processes, which could change chemical bonds or morphology of the surface. This has to be further investigated using different methods.

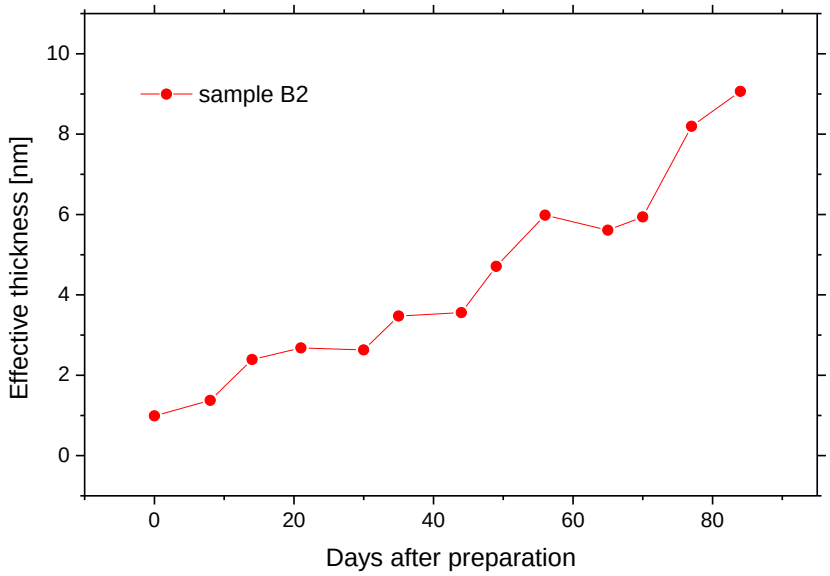

Figure 20: Time evolution of the effective thickness of sample B2 over 3 months.

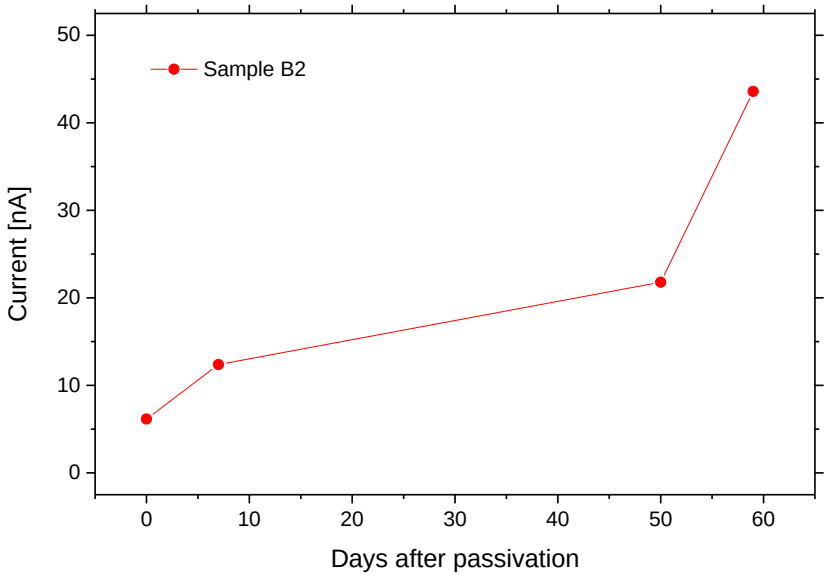

Figure 21: Time evolution of the leakage current at bias 400 V of sample B2 for up to 3 months.

5.4. NH_4F/H_2O_2 passivation

Sample C2 was treated with NH_4F solution for 2 minutes and was observed for up to 40 days. Again the EMA model with elemental tellurium and CdTe oxide was used. Multiple datasets analysis fit had the MSE of 2.6. The error in thickness and roughness was ± 0.5 nm.

Time evolution of the effective thickness and the current is depicted in Figure 22 and Figure 23, respectively. After surface treatment, the effective thickness was much larger (≈ 7.5 nm) with comparison to previous samples. During next several days there was a noticeable increase followed again by an approximately linear dependence on time. The leakage current was low already after the passivation, and decreased even more during the next 40 days. This passivation resulted in the growth of a thicker oxide surface layer that had low leakage currents and was stable during the observed period.

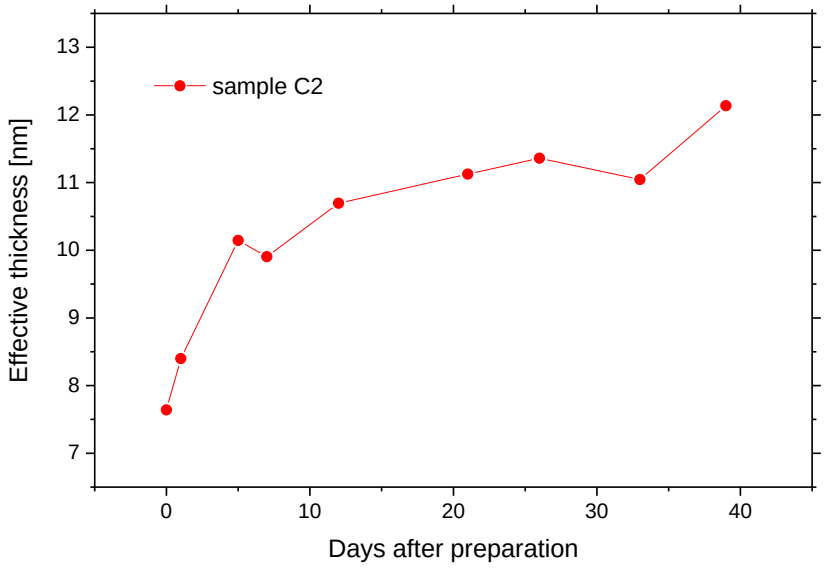

Figure 22: Time evolution of the effective thickness over 40 days of sample C2.

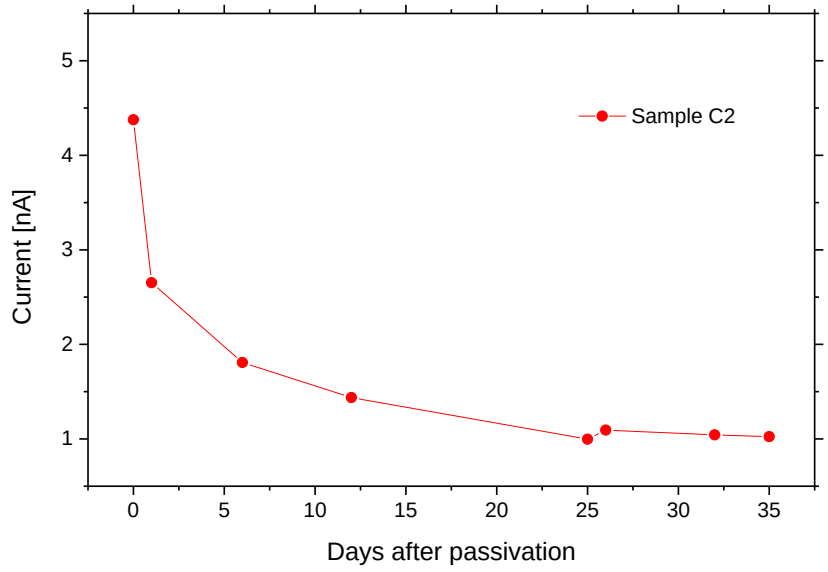

Figure 23: Time evolution of the current at bias 400 V over 40 days of sample C2.

5.5. Samples comparison

In Figure 24 the growth of the surface layers created by different passivation methods is compared. In Figure 25 is compared time evolution of leakage currents of all samples.

Thickest surface oxide layer is created by NH_4F solution 2 minutes treatment (sample C2). It is relatively stable when compared to other samples. Moreover, this sample shows best result in the leakage current measurements, specifically low initial values and decrease to 1 nA (at 400 V) after 40 days. 2 minutes KOH treatment also yields a well-behaved oxide surface layer, with less thick oxide layer and higher leakage currents with comparison to C2 sample. A1 sample has higher leakage currents during the semi-saturation period, when the oxide surface layer greatly grows in thickness. This surface is likely vulnerable to external conditions to which is exposed (air properties, mechanical damage etc.), mostly during the semi-saturation period. Therefore the properties of native oxide layer and its effects on the leakage currents can be undesirable. Then least satisfactory passivation method was 5 minute KOH passivation, which resulted in less thick layer and continuous increase in the leakage current.

There is a certain degree of correlation between ellipsometry and *I-V* characteristics: thicker surface oxide layer has lower leakage currents. However, the leakage current can be dependent on many properties of the material (resistivity, surface morphology and chemistry etc.) and cannot be explained only by properties indirectly determined by ellipsometry.

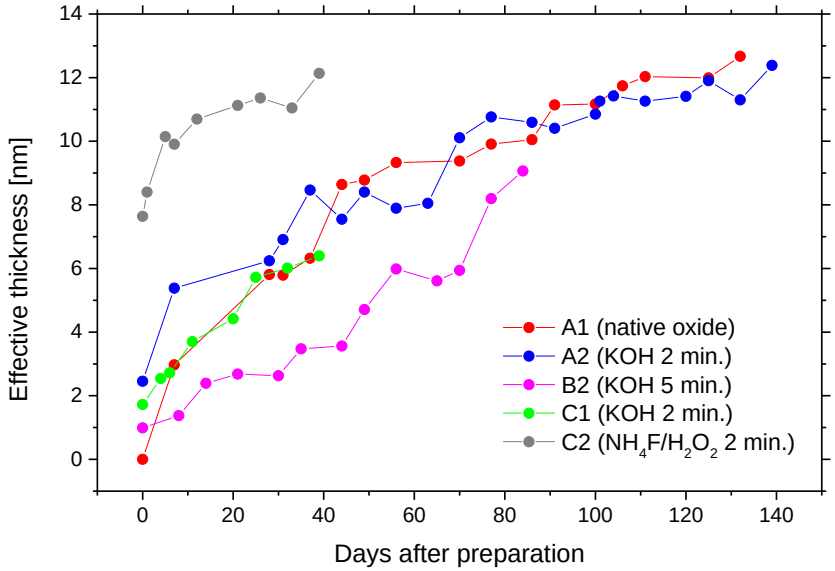

Figure 24: The growth of the surface oxide layer of all samples.

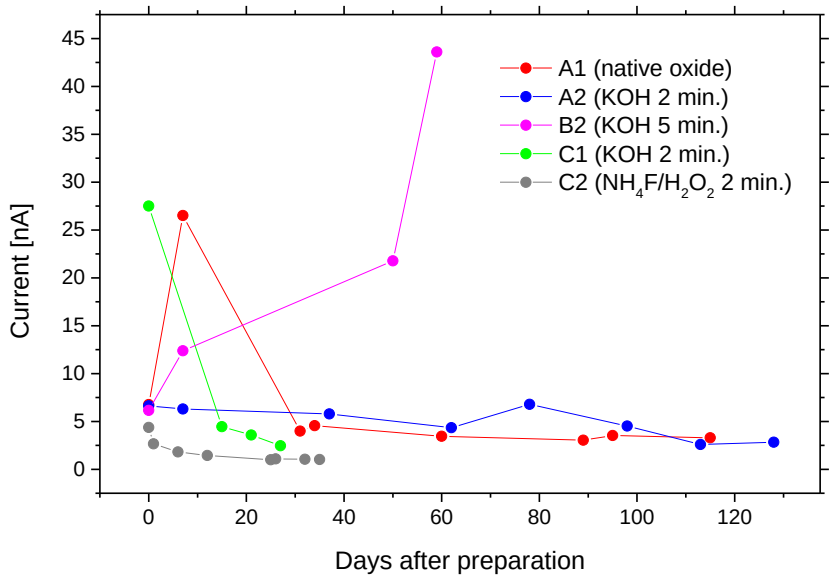

Figure 25: Time evolution of the leakage current at bias 400 V of all samples.

6. Conclusion

A group of CdZnTe samples was used to study growth of thin oxide layers. Native oxide surface and surfaces passivated by KOH (2 and 5 minutes treatments) and NH_4F/H_2O_2 (2 minutes treatment) were studied. Ellipsometry measurements showed change in *Del* and *Psi* parameters over time. Ellipsometric data were evaluated using the effective medium approximation model, which consisted of CdTe, CdTe oxide and elemental tellurium. Thickness and formation rate of the surface oxide layers differed in each of the passivation methods. A gradual increase in surface roughness over time was observed in all samples. Refractive index wavelength dependency of CdTe and CdTe oxide was determined in Lorentz and Cauchy approximations, respectively. XPS measurement was carried out and confirmed the growth of oxide bound to elemental tellurium. *I-V* characteristics were simultaneously measured over time. Samples exhibited various leakage current evolutions. NH_4F/H_2O_2 passivation showed to be method with most desirable properties of the surface oxide layer.

7. References

[1] T. E. Schlesinger et al., "Cadmium Zinc Telluride and its use as a Nuclear Radiation Detector Material," *Material Science and Engineering*, no. 32, pp. 103-189, 2001.

[2] Y. Cui, M. Groza, A. Burger, and R. B. James, "Effects of surface processing on the performance of CdZnTe Radiation detectors," *IEE Trans. Nucl. Sci.*, vol. 51, no. 3, pp. 1172-1175, June 2004.

[3] M.C. Duff et al., "Effects of surface preparation technique on the radiation detector perfomance of CdZnTe," *Applied Surface Science*, vol. 254, pp. 2889-2892, 2008.

[4] H. Bensalah et al., "The Effect of Etching Time on the CdZnTe Surface," *Applied Surface Science*, vol. 257, pp. 4633-4636, 2011.

[5] L. Marchini, A. Zapettini, and E. Gombia, "Study of Surface Treatment Effects on the Metal-CdZnTe Interface," *IEEE Trans. Nucl. Sci.*, vol. 56, no. 4, August 2009.

[6] A. Burger et al., "Characterization of metal contacts on surfaces of cadmium zinc telluride," *Nucl. Instruments Methods Phys. Res. Sect. A Accel. Spectrometers, Detect. Assoc. Equip.*, vol. 428, no. 1, pp. 8-13, June 1999.

[7] A.J. Nelson, A.M. Conway, C.E. Reinhardt, J.L. Ferreira, and S.A. Payne R.J. Nikolic, "X-ray photoemmision analysis of passivated CdZnTe surface for improved radiation detectors," *Materials letters*, vol. 63, pp. 180-181, 2009.

[8] V. A. Gnatyuk, O. I. Vlasenko, S. N. Levytskyi, J. Crocco, and H. Benselah, "Surface processing of CdZnTe crystals," *SPIE*, vol. 8507, p. 85071S, October 2012.

[9] J. Crocco et al., "Study of the effects of edge morphology on detector perfomance by leakage current and cathodoluminescence," *IEEE Transactions on Nuclear Science*, vol. 58, no. 4, pp. 1935-1941, 2011.

[10] A. Cavallini, A. Castaldini, D. Cavalcoli, and B. Fraboni, "Photocurrent and Surface Photovoltage Spectroscopy Investigations of CdTe-Based Compounds," *IEE Trans. Nucl. Sci*, vol. 54, no. 5, pp. 1719-1722, 2007.

[11] A. Hossain et al., "Effects of Surface Processing on the Response of CZT Gamma Detectors: Studies with a collimated synchrotron X-Ray Beam," *J. Electron. Mater.*, vol. 37, no. 9, pp. 1356-1361, March 3008.

[12] A. Bensouici et al., "Sutdy of effects of polishing and etching processes on Cd1-xZnxTe surface quality," *J. Cryst. Growth*, vol. 312, no. 14, pp. 2098-2102, July 2010.

[13] S. Tari et al., "Impact of Surface Treatment on the Structural and Electronic Properties of Polished CdZnTe Surfaces for Radiation Detectors," *J. Electron. Mater.*, vol. 42, no. 11, pp. 3252-3258, June 2013.

[14] S. S. Choi and G. Lucovsky, "Native Oxide Formation on CdTe," *Journal of Vacuum Science and Technology*, vol. 6, 1988.

[15] H.W. Yao, J.C. Erickson, and H.B. Barber, "Optical Properties of CdZnTe Studied by Variable Angle Spectroscopis Ellipsometry between 0.75 and 6.24 eV," *Journal of Electronic Materials*, vol. 28, no. 6, 1999.

[16] G. Badano, A. Million, and B. Canava, "Fast Detection of Precipitates and Oxides on CdZnTe Surfaces by Spectroscopic Ellipsometry," *Journal of Electronic Materials*, vol. 36, no. 8, 2007.

[17] J. Zázvorka et al., "Contactless resistivity and photoconductivity correlation to surface preparation of CdZnTe," *Appl. Surf. Sci*, vol. 315, pp. 144-148, October 2014.

[18] E. Wolf M. Born, *Principles of Optics: electromagnetic theory of propagation, interference and diffraction of light*, 5th ed. Oxford: Pergamon Press, 1975.

[19] J. Peatross and M. Ware. (2013) Physics of Light and Optics. Available at optics.byu.edu.

[20] Petr Malý, *Optika*. Prague: Karolinum, 2008.

[21] Harland G. Tompkins, *A user's guide to Ellipsometry*. New York: Dover Publications, inc., 2006.

[22] J. A. Woollam Co. [Online]. http://www.jawoollam.com/tutorial_5.html